HHS Public Access

Author manuscript

J Med Chem. Author manuscript; available in PMC 2022 April 13.

Published in final edited form as:

J Med Chem. 2021 November 11; 64(21): 15639–15650. doi:10.1021/acs.jmedchem.1c00697.

Multi-modal imaging probe for glypican-3 overexpressed in orthotopic hepatocellular carcinoma

Shuo Feng[1,§], **Xiaoqing Meng**[1,§], **Zhao Li**[5,§], **Tse-Shao Chang**[2], **Xiaoli Wu**[1], **Juan Zhou**[1], **Bishnu Joshi**[1], **Eun-Young Choi**[3], **Lili Zhao**[4], **Jiye Zhu**[5,*], **Thomas D. Wang**[1,2,6,*]

[1]Department of Medicine, Division of Gastroenterology, University of Michigan, Ann Arbor, MI 48109

[2]Department of Mechanical Engineering, University of Michigan, Ann Arbor, Michigan 48109

[3]Department of Pathology, University of Michigan, Ann Arbor, Michigan 48109

[4]Department of Biostatistics, University of Michigan, Ann Arbor, Michigan 48109

[5]Department of Hepatobiliary Surgery, Peking University People's Hospital, Beijing, China, 100044

[6]Department of Biomedical Engineering, University of Michigan, Ann Arbor, Michigan 48109

Abstract

Background & Aims: Hepatocellular carcinoma (HCC) is rising steadily in incidence, and more effective methods are needed for early detection and image-guided surgery. Glypican-3 (GPC3) is a cell surface biomarker that is overexpressed in early-stage cancer but not in cirrhosis. Peptides have small dimensions that can overcome delivery challenges, resulting in high concentration and deep penetration in tumor. We aim to demonstrate a peptide that is specific for GPC3, and validate specific uptake in a pre-clinical model of HCC.

Methods: We used phage display to biopan against purified GPC3 core protein to identify a candidate peptide, and used IRDye800 as a fluorescence label. The peptide was validated in vitro using knockdown, competition, and co-localization experiments. Binding parameters were measured. Specific peptide uptake by tumor was evaluated in orthotopically-implanted HCC tumors using photoacoustic and fluorescence imaging methods. Serum stability, peptide distribution and toxicity were characterized. Experiments were controlled using a scrambled peptide and indocyanine green.

[*]**Corresponding author**: Jiye Zhu, Ph.D., Professor of Department of Hepatobiliary Surgery, Peking University People's Hospital, Beijing, 100044, Office: (8610)88324176, Fax: (8610)88324175, gandanwk@vip.sina.com; Thomas D. Wang, M.D., Ph.D., Professor of Medicine, Biomedical Engineering, and Mechanical Engineering, H. Marvin Pollard Collegiate Professor of Endoscopy Research, Division of Gastroenterology, University of Michigan, 109 Zina Pitcher Pl. BSRB 1522, Ann Arbor, MI 48109-2200, Office: (734) 936-1228, Fax: (734) 647-7950, thomaswa@umich.edu.

[§]Authors contributed equally

Compliance with Ethical Standards

Declaration of Interest statement: JZ, BJ, ZL, and TDW are inventors on patents filed by the University of Michigan on the peptide presented. The authors declare that they have no known competing financial interests or personal relationships that could have appeared to influence the work reported in this paper.

Ethical approval: All applicable international, national, and/or institutional guidelines for the care and use of animals were followed. All human specimens used were deidentified tissues, thus no informed consent was required by the University of Michigan IRB.

Results: The 12-mer sequence ALLANHEELFQT was identified, and specific binding to GPC3 was validated in vitro. A binding affinity of k_d = 39.5 nM and time constant of k = 0.21 min^{-1} (4.76 min) were measured. Photoacoustic images showed peak tumor uptake at 1.5 hours post-injection, and clearance within ~24 hours. Laparoscopic images showed strong fluorescence intensity from tumor versus adjacent liver. The peptide was stable in serum with a half-life of 3.5 hours. Peptide biodistribution showed high uptake in tumor versus other organs. No acute peptide toxicity was observed on animal necropsy. Immunofluorescence staining of human liver specimens demonstrated specific binding to HCC versus cirrhosis, adenoma and normal liver.

Conclusions: A near-infrared peptide has demonstrated high affinity and fast kinetics for binding to GPC3, and specific uptake by orthotopically-implanted HCC tumors can be visualized in vivo using multi-modal imaging methods.

Hepatocellular carcinoma (HCC) is rising steadily in incidence, and more effective methods are needed for early detection and image-guided surgery. Glypican-3 (GPC3) is a cell surface biomarker that is overexpressed in early-stage cancer but not in cirrhosis. An IRDye800-labeled 12-mer sequence was identified, and specific binding to GPC3 was validated in vitro and in orthotopically-implanted HCC tumors in vivo. Over 4-fold greater binding affinity and 2-fold faster kinetics was measured by comparison with previous GPC3 peptides. Photoacoustic images showed peak tumor uptake at 1.5 hours post-injection and clearance within ~24 hours. Laparoscopic images and whole body fluorescence images showed strong intensity from tumor versus adjacent liver. Immunofluorescence staining of human liver specimens demonstrated specific binding to HCC versus cirrhosis, adenoma and normal liver. The near-infrared peptide demonstrated high affinity and fast kinetics for binding to GPC3, and specific uptake by orthotopically-implanted HCC tumors can be visualized in vivo using multi-modal imaging methods.

Keywords

hepatocellular carcinoma; glypican-3; peptide; imaging; fluorescence; near-infrared

Introduction

Hepatocellular carcinoma (HCC) is one of the most common causes of cancer-related deaths worldwide with >840,000 new cases each year,[1,2] and its contribution to the cancer burden in the U.S. is rapidly increasing.[3] HCC arises from cirrhosis, a sequalae of chronic hepatitis and an increasing prevalence of non-alcoholic fatty liver.[4–8] The steady growth of HCC demands more effective methods for early detection and therapy, in particular, for early-stage disease. Currently, α-fetoprotein (AFP) is used clinically as a serological biomarker for HCC surveillance, but is not useful as a tissue biomarker because of a low sensitivity of ~25%.[9] Furthermore, drug therapies for HCC have demonstrated only a minimal survival advantage over placebo.[10–12] Thus, new tissue biomarkers with high sensitivity and specificity for HCC are critically needed. Moreover, a targeting ligand that can be efficiently delivered to HCC tumor in vivo with specific uptake can be further developed to improve methods for image-guided surgery, distinguishing indeterminant liver nodules, and drug delivery.

Glypican-3 (GPC3), a member of the glypican family of heparan sulfate proteoglycans, is anchored via glycosylphosphatidylinositol (GPI) to the cell membrane.[13] The biochemical structure of GPC3 consists of a 70 kD core protein with two heparan sulfate side chains.[14] Overexpression of GPC3 stimulates the canonical Wnt signaling pathway to promote tumor growth, differentiation, and migration.[15,16] Increased gene transcription of GPC3 has been found in early-stage HCC (<2 cm).[17] Furthermore, high protein expression of GPC3 was found in small HCC tumors using immunohistochemistry (IHC),[18] and increased GPC3 immunostaining was observed in cirrhotic macronodules with malignant potential.[19] These results support GPC3 as a promising tissue biomarker for early-stage HCC. GPC3 is relatively absent in either normal liver or cirrhosis, and has expression levels that reflect tumor stage.[20–24] Furthermore, mutations in GPC3 and knockdown of function have been shown to inhibit HCC growth.[25]

Peptide-based ligands have properties that are well matched for in vivo delivery to tumors that arise from cirrhotic livers.[26–28] Their small size and low molecular weight facilitate challenging navigation obstacles, including irregular microvasculature, heterogeneous uptake, and transport barriers.[29–36] Peptides can diffuse and extravasate through leaky vessels to achieve high concentrations and deep penetration in solid tumors. Also, peptides have low potential for immunogenicity.[37,38] Established peptide synthesis processes are easy to scale up for mass production with reproducible products at low cost.[39,40] By comparison, antibodies are much larger in size, which limits their ability to extravasate from the vasculature, diffuse and penetrate into tumor, and clear from interstitial space.[41–44] Peak uptake in tumor typically takes 2–3 days, and antibodies are prone to immunogenicity, which can limit repeat use.[45] Here, we aim to identify and validate a peptide specific for GPC3, and using a near-infrared (NIR) label, demonstrate feasibility to target HCC in vivo using multi-modal imaging.

Results

Identification of GPC3 as HCC target

Gene expression profiles from human HCC specimens were analyzed from 2 independent datasets, GSE14520 and GSE44074, Fig. S1A,B.[46,47] GPC3 showed large differences in average fold-change (Δ) for HCC tumor by comparison with non-tumor. The data points are shown on log scale, Fig. S1C,D. The ROC curve for GSE14520 shows 87% sensitivity and 90% specificity with an area-under-the curve (AUC) of 0.92, Fig. S1E.

GPC3 expression in HCC was supported by results using immunohistochemistry (IHC). On representative sections of human HCC, no staining was observed for normal, minimal reactivity was seen for adenoma, and mild staining was found for cirrhosis, Fig. S2A–C. Either strong or moderate reactivity occurred with n = 22 out of 25 specimens of HCC (88% positives), Fig. S2D. Histology performed on adjacent sections is shown, Fig. S2E–H. An expert liver pathologist evaluated the specimens using a standard IHC scoring system.

Peptide specific for GPC3

Peptide selection was performed by biopanning a phage display library against purified recombinant GPC3 core protein. After 4 rounds, the 12-mer peptide with sequence ALLANHEELFQT was identified based on enrichment. This peptide (black) was synthesized and attached to a IRDye800 (red) fluorophore via a GGGSC linker (blue) on the C-terminus to prevent steric hindrance, hereafter ALL*-IRDye800, Fig. 1A. IRDye800 was chosen for its high quantum yield and photostability.[48] The scrambled sequence FEAEHNLALQTL was labeled with IRDye800 for use as control, hereafter FEA*-IRDye800, Fig. 1B. 3D space filling models show the structural differences between these 2 peptides. The absorbance and fluorescence emission spectra peak at λ_{abs} = 775 nm and λ_{em} = 816 nm, respectively, Fig. 1C,D. The IRDye800-labeled peptides were purified to >95% by HPLC, and an experimental mass-to-charge (m/z) ratio of 2870.09 was measured using mass spectrometry for ALL*-IRDye800 and FEA*-IRDye800, agreeing with expected values, Fig. S3A,B.

GPC3 knockdown in HCC cells

Strong binding by ALL*-IRDye800 (red) and AF488-labeled anti-GPC3 (green) was observed at the surface (arrow) of Hep3B cells transfected with siCL non-targeting siRNA (control), Fig. 2A. Minimal signal was seen with either peptide or antibody for Hep3B knockdown cells transfected with 3 unique siRNAs, Fig. 2B–D. Quantified results showed significantly reduced fluorescence intensity with peptide and antibody in all GPC3 knockdown cells, Fig. 2E. Also, signal from ALL*-IRDye800 was significantly greater than that from FEA*-IRDye800. Western blot shows GPC3 expression for the control and knockdown cells, Fig. 2F.

Competition for peptide binding

Unlabeled ALL* was added to compete for binding (block) with ALL*-IRDye800 to Hep3B cells, and significantly reduced fluorescence intensities were observed in a concentration dependent manner, Fig. 3A. The addition of unlabeled FEA* (control) showed no significant changes, Fig. 3B. The fluorescence intensities were quantified, and the differences for ALL* and FEA* were found to be significant at concentrations of 50 μM and greater, Fig. 3C. These results support the peptide rather than the fluorophore mediating specific binding interactions with the GPC3 target.

Co-localization of peptide and antibody binding

Strong fluorescence from ALL*-IRDye800 (red) and AF488-labeled anti-GPC3 (green) was observed on the surface of Hep3B cells using confocal microscopy, Fig. 3D. The merged image showed co-localization of peptide and antibody binding with a correlation of ρ = 0.71.

Characterization of peptide binding

An apparent dissociation constant of k_d = 39.5 nM, and an apparent association time constant of k = 0. 21 min^{-1} (4.8 min) were measured for ALL*-IRDye800 binding to Hep3B cells using flow cytometry, Fig. 3E,F. These results support binding with high affinity and rapid onset, respectively.

In vivo photoacoustic imaging of orthotopic human HCC xenograft tumors

Photoacoustic images were collected in vivo from mice bearing orthotopically-implanted human Hep3B HCC xenograft tumors to evaluate the time course for peptide uptake. Minimal intensity was seen from the tumors prior to peptide injection (0 hour). ALL*-IRDye800 (150 μM, 200 μL), FEA*-IRDye800 (150 μM, 200 μL), ALL* (block, 1.5 mM, 100 μL), and ICG (2.46 mg/kg) were administered intravenously, and images were collected over 48 hours, Fig.4A–D. Blocking was performed by injecting unlabeled ALL* prior to ALL*-IRDye800 to block binding interactions and serve as an additional control. Quantified intensities showed a peak T/B ratio at 1.5 hours after injection of ALL*-IRDye800, Fig. 4E. By comparison, ICG did not reach peak uptake until over 48 hours post-injection. This difference can be explained by the non-specific, passive accumulation of ICG in HCC via the EPR effect.[49] The signal decreased to the baseline by ~24 hours post-injection. The mean value at 1.5 hours was significantly greater for ALL*-IRDye800 versus FEA*-IRDye800, ALL* (block), and ICG, Fig. 4F.

In vivo laparoscopic imaging of orthotopic human HCC xenograft tumors

An ultrasound and T_1-weighted MR image were collected from a representative mice to confirm orthotopic implantation of HCC tumor (arrow) in the liver, Fig. 5A,B. ALL*-IRDye800, FEA*-IRDye800, ALL* (block), and ICG were administered systemically 1.5 hours prior to imaging. Representative white light (WL) and fluorescence (FL) images collected in vivo from the exposed liver are shown, Fig. 5C,D. A conventional surgical laparoscope was attached to an imaging module to collect white light and NIR fluorescence images, Fig. S4. Image intensities were quantified, and the mean T/B ratio for ALL*-IRDye800 was found to be significantly greater than that for FEA*-IRDye800, ALL* (block), and ICG, Fig. 5E. Moreover, ALL*-IRDye800 produced sharp tumor margins (arrows) by comparison with ICG.

After imaging was completed, the mice were euthanized, and the livers were resected, formalin-fixed, and sectioned. Immunohistochemistry was performed using an anti-cytokeratin specific for human tissues, and showed reactivity in the human HCC tumor implanted in mouse liver, Fig. 5F. Strong staining with anti-GPC3 confirmed GPC3 expression in HCC, Fig. 5G. Bright fluorescence was observed on the cell surface of HCC using anti-GPC3-AF488, Fig. 5H. Representative histology (H&E) of the tumor is shown, Fig. 5I.

In vivo whole body NIR fluorescence imaging of orthotopic human HCC xenograft tumors

Whole body NIR fluorescence images were collected in vivo to validate specific peptide uptake in the orthotopically-implanted HCC tumors. ALL*-IRDye800, FEA*-IRDye800, ALL* (block), and ICG were administered intravenously 1.5 hours prior to imaging. Representative fluorescence images are shown, Fig. 6A–D. Image intensities were quantified, and the mean T/B ratio was found to be significantly greater for ALL*-IRDye800 than that for FEA*-IRDye800, ALL* (block), and ICG, Fig. 6E.

Serum stability

The stability of ALL*-IRDye800 in mouse serum was evaluated using analytical RP-HPLC. The relative concentration was determined by the area under the peak, and a half-life of $T_{1/2}$ = 3.5 hours was measured, R^2 = 0.99, Fig. 6F.

Peptide biodistribution

HCC tumor-bearing mice were injected with ALL*-IRDye800, FEA*-IRDye800, ALL* (block), and ICG. The animals were euthanized 1.5 hours later. Major organs, including liver, spleen, kidney, stomach, intestine, heart, lung, and brain, were resected, and NIR fluorescence images were collected, Fig. S5A–D. Strong signal was observed from tumor for ALL*-IRDye800 by comparison with FEA*-IRDye800, ALL* (block), and ICG. The fluorescence intensities were quantified, and the mean (±SD) intensity from tumor was significantly greater for ALL*-IRDye800 versus FEA*-IRDye800, ALL* (block), and ICG, Fig. S5E. Also, the mean signal for ALL*-IRDye800 is significantly higher for tumor versus adjacent liver. Strong signal was observed from the kidneys for the animals injected with peptides versus ICG to support renal clearance.

Animal necropsy

Normal healthy mice were sacrificed 48 hours after injection of ALL*-IRDye800. Vital organs were evaluated by histology. No signs of acute peptide toxicity were seen in brain, heart, lung, liver, spleen, kidney, stomach, intestine, cecum, colon, Fig. S6A. Whole blood and serum were collected for evaluation of hematology and chemistry, and no acute peptide toxicity was observed, Fig. S6B,C.

Ex vivo microscopy of human HCC specimens

Formalin-fixed, paraffin-embedded (FFPE) specimens of human liver were obtained from the archived tissue bank in the Department of Pathology at the University of Michigan. Immunofluorescence using ALL*-IRDye800 (red) and anti-GPC3-AF488 (green) showed negligible staining to a representative section of normal human liver, Fig. 7A. Peptide and antibody showed minimal staining to adenoma and moderate diffuse staining to cirrhosis, Fig. 7B,C. Intense staining is observed for HCC, Fig. 7D. Results were compared with histology interpreted by an expert liver pathologist (EYC). From the merged images, a Pearson's correlation coefficient of ρ = 0.68, 0.82, 0.72, and 0.74, respectively, were calculated to evaluate co-localization of antibody and peptide binding. The fluorescence intensities were quantified, and the mean (±SD) values were significantly greater for HCC than for the other histological classifications, Fig. 7E. The ROC curve shows 81% sensitivity and 84% specificity for distinguishing HCC from all non-HCC with AUC = 0.90, Fig. 7F, and 79% sensitivity and 79% specificity for distinguishing HCC from cirrhosis with AUC = 0.80, Fig. 7G.

Discussion and conclusion

Here, we used phage display methods against purified core GPC3 protein to identify a 12-mer peptide specific for this target. GPC3 was found in gene expression profiles to be highly overexpressed in human HCC versus non-tumor,[46,47] and increased protein expression was

supported by immunohistochemistry. After labeling the peptide with IRDye800, specific binding was validated by knockdown, competition, and co-localization studies. In vitro binding was characterized by parameters that support high binding affinity and rapid onset. Hep3B xenograft tumors were orthotopically-implanted in immunocompromised mice, and peak in vivo uptake by xenograft tumor was observed at 1.5 hours post-injection using photoacoustic imaging. Specific peptide uptake was supported by fluorescence images collected in vivo using a NIR laparoscope. The mean fluorescence intensity for ALL*-IRDye800 was significantly greater than that for FEA*-IRDye800 (control), ALL* (block), and ICG (non-specific). These results were confirmed with in vivo whole body NIR fluorescence images. The peptide was found to be stable in serum with a half-life of $T_{1/2}$ = 3.5 hours. No evidence of toxicity was observed on animal necropsy. High sensitivity and specificity for distinguishing HCC from cirrhosis were found by staining human HCC sections.

Our rigorous selection and validation process has resulted in a peptide with over 4-fold greater binding affinity and 2-fold faster kinetics by comparison with previous GPC3 peptides. Previously, a 12-mer was identified using phage display methods, and was labeled with Cy5.5.[50] A k_d = 735.2±53.6 nM to recombinant GPC3 protein was reported. In vivo fluorescence images showed peak uptake at 4 hours post-injection and significantly higher accumulation in HepG2 (GPC3+) xenograft tumors versus control. This peptide was also used to visualize GPC3 expression in human HCC specimens ex vivo. Another study used the same approach, and identified a different sequence with k_d = 280.4±33.5 nM.[51] Also, a 14-mer was identified using mass spectrometry analysis, and labeled with FITC.[52] Specific binding to GPC3 by this peptide and a 7-mer variant was demonstrated with HepG2 cells using fluorescence microscopy and competition experiments. Binding affinity and kinetics properties were not reported.

In this study, we used photoacoustic and fluorescence imaging methods to validate specific peptide uptake by HCC in vivo. This multi-modal imaging approach uses the physical properties of one modality to confirm the results of another, and provides a rigorous validation strategy whereby the IRDye800 label was used to generate both fluorescence and photoacoustic signal. This NIR fluorophore provides a complementary approach to visualize, monitor, and characterize properties for peptide delivery to tumor in vivo. Photoacoustic imaging combines light excitation with sound detection, and was used to evaluate the time course of peptide uptake following intravenous administration. Fluorescence provides images with a large field-of-view (FOV). This feature was used to localize the margins of HCC tumor within the liver and to assess the systemic biodistribution of the contrast agent. In addition, ultrasound and MRI were used to confirm orthotopic implantation of the HCC tumor.

Surgical resection is playing in increasing role in the management of HCC patients, in particular, for isolated lesions in those who cannot receive a liver transplant. Image-guided surgery is being used by hepatobiliary surgeons with greater frequency to more precisely resect HCC. Currently, ICG is an FDA-approved contrast agent that is being used with intravenous injection to identify liver tumors, hepatic segments, and extrahepatic bile ducts in real time during open and laparoscopic surgery.[53–55] This non-specific NIR fluorophore

accumulates passively in HCC via the enhanced permeability and retention (EPR) effect.[56] Our results showed that ICG achieves peak uptake over 48 hours post-injection by comparison with 1.5 hours for the NIR-labeled peptide. Moreover, laparoscopic images showed indistinct tumor margins for ICG versus our NIR-labeled peptide. The intraoperative diagnosis of small tumors, especially those with indistinct margins, remains an important challenge for HCC resection. Thus, a specific targeting agent has potential to significantly improve diagnostic performance.

Clinical translation of this targeting ligand is needed to validate specific peptide uptake in human HCC tumor. While we demonstrated this property in a pre-clinical model, the HCC tumor was orthotopically-implanted in a normal rather than cirrhotic liver, which would likely present unique delivery challenges. Laparoscopy can be used to visualize fluorescence from early-stage tumors (<2 cm) to identify lesions missed by conventional white light illumination. In addition, tissues can be resected to validate GPC3 expression and selective peptide uptake. This NIR-labeled peptide will likely be safe in human subjects with intravenous administration. IRDye800 has been previously used to label a 14mer specific for the gastrin-releasing peptide receptor (GRPR), and was used safely for image-guided surgery of glioblastoma multiforme in n = 29 human subjects.[57] A validated ligand specific for GPC3 can then be developed for broad clinical use to improve management of HCC patients, including image-guided surgery, distinguishing indeterminant liver nodules, and labeling drug carriers.

Methods

Cells, media, and chemicals

Human Hep3B HCC cells were purchased from the ATCC. All cell lines were cultured in Eagle's Minimum Essential Medium (EMEM) with 10% fetal bovine serum (FBS), 1% sodium pyruvate, and 1% MEM non-essential amino acids solution at 37°C with 5% CO_2. All media and reagents were purchased from Gibco.

Phosphine HCl (TCEP) was obtained from Sigma-Aldrich. IRDye800CW maleimide was procured from LI-COR Biosciences. Acetonitrile was ordered from Fisher Scientific. Peptides were synthesized by BIOMATIK with purity over 95% by HPLC. All chemicals were of analytical grade, and used without further purification.

Peptide specific for GPC3

Purified human recombinant GPC3 core protein (62 kDa, Sino Biological Inc) was immobilized in a 6-well plate. An M13 bacteriophage library (Ph.D.™−12, New England Biolabs Inc) with $>10^9$ unique sequences was used to perform 4 rounds of biopanning with decreasing quantity (100, 80, 60, and 40 μg) of GPC3 core protein at 4°C. After the 4th round, 50 plaques were randomly selected for DNA preparation and sequence analysis. Enriched phages were amplified, and purified.

Peptides (2 mg) were dissolved in 2 mL of coupling buffer (0.1 M sodium phosphate, 0.5 mM TCEP, pH 7.4). IRDye800CW maleimide (1 mg) was added, and the reaction was performed under N_2 for 2 hours at room temperature, hereafter RT. The resulting

peptides were then purified using reversed-phase high performance liquid chromatography (RP-HPLC) and characterized with mass spectrometry. Peptide purity was evaluated using an analytical C18-column.

The absorbance spectra of the IRDye800-labeled peptides were measured at a concentration of 10 μM using a UV-Vis spectrophotometer (NanoDrop 2000, Thermo Scientific). Fluorescence emission spectra were measured using a fiber-coupled spectrophotometer (USB2000+, Ocean Optics) with a laser excitation at λ_{ex} = 785 nm provided by a solid state diode laser (#iBEAM-SMART-785-S, Toptica Photonics). The spectra were plotted using GraphPad Prism 8 software.

GPC3 knockdown in HCC cells

Knockdown of GPC3 was performed in Hep3B cells using 3 unique GPC3 siRNAs (#14657, #14750, and #14836, Thermo Fisher Scientific), and a negative control siRNA (MISSION® siRNA Universal Negative Control #1, Sigma-Aldrich). The cells were seeded in 6-well plates at ~70% confluence in EMEM supplemented with 10% FBS without antibiotics or other supplements. The cells were transfected with 5 nmol siRNA using lipofectamine 3000 (Thermo Fisher Scientific). Knockdown efficiency was confirmed by Western blot. Cells were first washed in PBS and then lysed using RIPA solution (Thermo Fisher Scientific). Aliquots were placed on ice for 30 min, centrifuged at 14,000 rpm for 10 min at 4°C, and the supernatants were collected. Protein concentrations were determined using a BCA assay kit (23225, Thermo Scientific). Western blot was performed using a 1:1000 dilution of primary monoclonal rabbit anti-GPC3 antibody (#SP86, Abcam Inc). Loading was controlled with a 1:1000 dilution of mouse anti-GAPDH antibody (#D4C6R, Cell Signaling Technology). Western blot membrane was developed by chemiluminescent substrate (GE Healthcare), and detected with X-ray film (Denville Scientific).

Hep3B cells were grown on coverslips to ~100% confluence, washed with PBS, and fixed with cold methanol for 5 min. The cells were incubated with 5 μM of the IRDye800-labeled peptides for 5 min at RT. The cells were washed 3X in PBS, and mounted on glass slides with ProLong Gold reagent containing DAPI (Invitrogen). Fluorescence images were collected using a confocal microscope (Leica SP5 Inverted Confocal Microscope) at λ_{em} = 690–800 nm with λ_{ex} = 670 nm excitation, and were quantified using NIH ImaFgeJ software. For antibody staining, the cells were washed 3X in PBS, fixed with cold methanol for 5 min and blocked in 2% BSA for 30 min at RT. The cells were incubated with 1:200 dilution of anti-GPC3 antibody (SP86, Abcam Inc) with 2% BSA overnight at 4°C. The cells were washed 3X with PBS and processed for secondary staining. Goat anti-rabbit antibody labeled with 1:500 Alexa-Fluor 488 (AF488, Invitrogen) with 2% BSA was added to the cells and incubated for 1 hour at RT. Cells were further washed 3X with PBS and mounted on glass cover slips with ProLong Gold reagent containing DAPI. Fluorescence images were collected using a confocal microscope (Leica SP5 Inverted Confocal Microscope) at λ_{em} = 510–650 nm with λ_{ex} = 488 nm excitation, and were quantified using NIH ImageJ software.

Competition for peptide binding

Hep3B cells were grown to ~100% confluence on cover slips. The cells were washed with PBS 3X and fixed with cold methanol for 5 min. Unlabeled peptides at concentrations of 0, 50, 100, 150 and 200 μM were added to the cells and incubated for 30 min at RT. The cells were then washed with PBS 3X, and further incubated with 5 μM of IRDye800-labeled peptides for another 30 min at 4°C. The cells were washed again with PBS, and mounted with ProLong Gold reagent containing DAPI (Invitrogen).

Characterization of peptide binding

The apparent dissociation constant was measured by incubating ~10^6 Hep3B cells with different concentrations of IRDye800 labeled peptide ranging between 0–200 nM at 25°C for 1 hour, and washed with cold PBS. The mean fluorescence intensities were measured with flow cytometry (BD LSR Fortessa, BD Biosciences). The equilibrium dissociation constant $k_d = 1/k_a$ was calculated by performing a least squares fit of the data to the non-linear equation $I = (I_0+I_{max}k_a[X])/(I_0+k_a[X])$.[58] I_0 and I_{max} are the initial and maximum fluorescence intensities, corresponding to no peptide and at saturation, respectively. [X] represents the concentration of bound peptides. Graphpad Prism ver 8 software was used to plot and fit the data.

The apparent association time constant k was measured by incubating ~10^6 Hep3B cells with 5 μM of IRDye800-labeled peptides at time intervals between 0–40 min at 25°C. The cells were centrifuged and washed with cold PBS. Flow cytometry was performed using Sony iCyt SY3200 at λ_{em} = 775/50 nm with λ_{ex} = 685 nm excitation, and the median fluorescence intensity (y) was ratioed with that found without peptide at different time points (t) using Flowjo (ver 10.1r5) software. The rate constant k was calculated by fitting the data to a first order kinetics model, $y(t) = I_{max}[1\text{-}exp^{(-kt)}]$, where I_{max} = maximum value.[59]

Orthotopically-implanted human Hep3B HCC xenograft tumors

All experimental procedures were performed in accordance with relevant guidelines and regulations of the University of Michigan. All animal studies were conducted with approval by the University Committee on the Use and Care of Animals (UCUCA). Animals were housed per guidelines of the Unit for Laboratory Animal Medicine (ULAM). Anesthesia was induced and maintained via a nose cone with inhaled isoflurane mixed with oxygen at a concentration of 2–4% and flow rate of ~0.5 L/min. Hep3B cells were grown to ~90% confluence and diluted in growth factor reduced (GFR) Matrigel Matrix (Corning). Nude athymic mice (nu/nu, Jackson Laboratory) at 4–6 weeks of age with weights between 20–25 grams were used. A small incision was made below the sternum to expose the liver, and a pellet of ~1×10^6 Hep3B cells in 50 μL PBS and matrigel matrix mixture (1:1) was slowly injected into the upper region of the left lobe of the liver using a 27-gauge needle. The surgical incision was closed with sutures (#J385H, VICRYL, 5–0) and wound clips (9 mm EZ Clip, Braintree Scientific).

In vivo photoacoustic imaging of HCC orthotopic tumors

The IRDye800-labeled peptides (150 μM in 200 μL of PBS) were injected in mice bearing orthotopically-implanted human Hep3B HCC xenograft tumors. Unlabeled peptide (1.5 mM in 100 μL of distilled water) was injected 30 min prior to the labeled peptide to compete for binding. ICG (2.46 mg/kg) was injected intravenously as control. Photoacoustic images were collected from 0–48 hours post injection (Nexus128, Endra Inc) using λ_{ex} = 774 nm excitation. Mice were placed prone in a plastic tray with the tumor facing the water-filled dimple for acoustic coupling. The images were collected with 120 views at 20 pulses/view. Each image covered a volume of 25×25×25 mm^3 with a voxel size of 280 μm^3. Images were viewed and analyzed using OsiriX image processing software.

Ultrasound imaging of HCC orthotopic tumors

Tumor dimensions were measured using ultrasound (SonixTablet, Ultrasonix Medical Corporation). The mice were placed on a heated pad. Ultrasound gel (Aquasonic 100, Parker Laboratories) was applied to the external skin. A linear transducer (L40–8/12) was used. Each image had a 12 × 12 mm^2 field-of-view (FOV) with an in-plane pixel resolution of 50 × 50 μm^2.

MRI imaging of HCC orthotopic tumors

T_1-weighted MR images were collected from mice using a 7T horizontal bore small animal magnet (SGRAD 205/120/HD/S, Agilent Technologies). The feedback control system maintained the core mouse body temperature at 37°C by blowing hot air into the magnet. The parameters of MR images include orientation = axial, echo time (TE): 10 ms, repetition time (TR): 717 ms, average = 4, slices = 35, thickness = 0.5 mm, and display matrix (RO×PE) = 256×128.

Laparoscopic imaging of HCC orthotopic tumors

A standard surgical laparoscope (#49003 AA, HOPKINS® II Straight Forward Telescope 0°, Karl Storz) was adapted to collect NIR fluorescence images. White light illumination (MCWHL5, Thorlabs) and laser excitation at λ_{ex} = 785 nm were coupled into the laparoscope via a liquid light guide (LLG3–4Z, Thorlabs). White light images were collected by a color CCD camera (#GX-FW-28S5C-C, Point Grey Research) at 30 frames per second. Fluorescence images were collected by a NIR sensitive CCD camera (Orca R-2, Hamamatsu Photonic) at 10 frames per second using a laser power of 1.2 mW.

Whole body fluorescence imaging of HCC orthotopic tumors

A small (1–2 cm) incision was made in the abdomen below the sternum in mice with orthotopically implanted human Hep3B HCC xenograft tumors to expose the liver. The IRDye800-labeled peptides, unlabeled ALL* (block), and ICG were injected via tail vein, as described above. Whole body NIR fluorescence images were collected using the Pearl Trilogy (LI-COR Biosciences) with λ_{ex} = 785 nm excitation and λ_{em} = 820 nm emission. Fluorescence intensities are quantified using Image Studio software. Regions of normal liver adjacent to the tumor was used as background.

Immunohistochemistry (IHC) of HCC orthotopic tumors

Formalin-fixed, paraffin-embedded (FFPE) sections were deparaffinized and antigen unmasking was performed using a standard protocol.[60] Sections were incubated with a 1:200 dilution of mouse anti-human cytokeratin (#CAM5.2, BD Biosciences) and rabbit anti-GPC3 antibody (#SP86, Abcam) or at 4°C overnight. VECTASTAIN® Elite ABC-HRP Kit (#PK-6101 rabbit IgG or #PK-6102 mouse IgG) was then applied. Adjacent sections were processed for routine histology (H&E).

Serum stability

Mouse serum was incubated with the IRDye800-labeled peptide (15 μM) at time intervals ranging up to 24 hours at 37°C. Samples were precipitated by adding a double volume of acetonitrile and centrifuging for 10 min at 4°C. The supernatants were stored at −80°C. Serum stability was monitored by analytical RP-HPLC. The relative peptide concentration was determined by measuring the area-under-the-peak.

Peptide biodistribution

The IRDye800-labeled peptides, unlabeled ALL* (block), and ICG were injected via tail vein into normal healthy mice, as described above. The mice were euthanized at 1.5 hours post-injection. The tumor and major organs, including spleen, kidney, stomach, liver, intestine, heart, lung and brain, were excised and imaged using the Pearl Trilogy (LI-COR Biosciences) with excitation at λ_{ex} = 785 nm and emission at λ_{em} = 820 nm. Fluorescence intensities were quantified using Image Studio software.

Animal necropsy

Healthy mice were euthanized 48 hours after intravenous injection of the IRDye800-labeled peptide. Whole blood (~600 μL) was collected immediately by cardiac puncture, and submitted for chemistry. Major organs, including liver, kidney, heart, lung, spleen, stomach, intestine and brain were resected and processed for routine histology (H&E). All slides were evaluated by an expert liver pathologist (EYC).

Ex vivo microscopy of human HCC specimens

All experiments performed using human tissues were approved by the Michigan Medicine IRB (HUM00122873). Formalin-fixed, paraffin-embedded (FFPE) specimens of human liver were obtained from the archived tissue bank of the Department of Pathology. The specimens were cut in 5 μm thick sections, and mounted onto glass slides (Superfrost Plus, Fischer Scientific). The tissues were deparaffinized, and antigen retrieval was performed.[60] The sections were blocked with goat serum for 30 min at RT, and incubated with 1:200 dilution of anti-GPC3 antibody (#SP86, Abcam) overnight at 4°C and 1:500 AF488-labeled goat anti-rabbit secondary antibody (#A-11029, Life Technologies). The slides were stained with the IRDye800-labeled peptide at 5 μM concentration for 10 min at RT. The sections are washed 3X with PBST and mounted with Prolong Gold reagent containing DAPI (Invitrogen). The fluorescence images were collected using Zeiss Apotome (upright), excitation at λ_{ex} = 685 nm for peptide and λ_{ex} = 485 nm for antibody. Fluorescence

intensities were quantified using custom Matlab software (Mathworks). Regions of saturated intensities were avoided. All slides were evaluated by an expert liver pathologist (EYC).

Supplementary Material

Refer to Web version on PubMed Central for supplementary material.

Funding:

This study was funded in part by the National Institutes of Health U01 CA230669 (TW) and the UMHS-PUHSC Joint Institute (JZ,TW).

Abbreviations

FOV	field-of-view
GPC3	glypican-3
HCC	hepatocellular carcinoma
H&E	hematoxylin & eosin
ICG	indocyanine green
IHC	immunohistochemistry
NIR	near infrared
T/B	target-to-background

References

1. Bray F, Ferlay J, Soerjomataram I, Siegel RL, Torre LA, Jemal A. Global cancer statistics 2018: GLOBOCAN estimates of incidence and mortality worldwide for 36 cancers in 185 countries. CA Cancer J Clin 2018;68:394–424. [PubMed: 30207593]
2. Siegel RL, Miller KD, Jemal A. Cancer statistics, 2020. CA Cancer J Clin 2020;70:7–30. [PubMed: 31912902]
3. Peery AF, Crockett SD, Murphy CC, Lund JL, Dellon ES, Williams JL, Jensen ET, Shaheen NJ, Barritt AS, Lieber SR, Kochar B, Barnes EL, Fan YC, Pate V, Galanko J, Baron TH, Sandler RS. Burden and Cost of Gastrointestinal, Liver, and Pancreatic Diseases in the United States: Update 2018. Gastroenterology 2019;156:254–272.e11. [PubMed: 30315778]
4. Chemin I, Zoulim F. Hepatitis B virus induced hepatocellular carcinoma. Cancer Lett 2009;286:52–9. [PubMed: 19147276]
5. Hoshida Y, Fuchs BC, Bardeesy N, Baumert TF, Chung RT. Pathogenesis and prevention of hepatitis C virus induced hepatocellular carcinoma. J Hepatol 2014;61(S1):S79–S90. [PubMed: 25443348]
6. Klein S, Dufour JF. Nonalcoholic fatty liver disease and hepatocellular carcinoma. Hepat Oncol 2017;4:83–98. [PubMed: 30191057]
7. Kutlu O, Kaleli HN, Ozer E. Molecular Pathogenesis of Nonalcoholic Steatohepatitis- (NASH-) Related Hepatocellular Carcinoma. Can J Gastroenterol Hepatol 2018;2018:8543763. [PubMed: 30228976]
8. Schlesinger S, Aleksandrova K, Pischon T, Fedirko V, Jenab M, Trepo E, Boffetta P, Dahm CC, Overvad K, Tjønneland A, Halkjær J, Fagherazzi G, Boutron-Ruault MC, Carbonnel F, Kaaks R, Lukanova A, Boeing H, Trichopoulou A, Bamia C, Lagiou P, Palli D, Grioni S, Panico S, Tumino R, Vineis P, Bueno-de-Mesquita HB, van den Berg S, Peeters PH, Braaten T, Weiderpass

E, Quirós JR, Travier N, Sánchez MJ, Navarro C, Barricarte A, Dorronsoro M, Lindkvist B, Regner S, Werner M, Sund M, Khaw KT, Wareham N, Travis RC, Norat T, Wark PA, Riboli E, Nöthlings U. Abdominal obesity, weight gain during adulthood and risk of liver and biliary tract cancer in a European cohort. Int J Cancer 2013;132:645–57. [PubMed: 22618881]

9. International Consensus Group for Hepatocellular NeoplasiaThe International Consensus Group for Hepatocellular Neoplasia. Pathologic diagnosis of early hepatocellular carcinoma: a report of the international consensus group for hepatocellular neoplasia. Hepatology 2009;49:658–64. [PubMed: 19177576]
10. Bangaru S, Marrero JA, Singal AG. Review article: new therapeutic interventions for advanced hepatocellular carcinoma. Aliment Pharmacol Ther 2020;51:78–89. [PubMed: 31747082]
11. Llovet JM, Ricci S, Mazzaferro V, Hilgard P, Gane E, Blanc JF, de Oliveira AC, Santoro A, Raoul JL, Forner A, Schwartz M, Porta C, Zeuzem S, Bolondi L, Greten TF, Galle PR, Seitz JF, Borbath I, Häussinger D, Giannaris T, Shan M, Moscovici M, Voliotis D, Bruix J; SHARP Investigators Study Group. Sorafenib in advanced hepatocellular carcinoma. N Engl J Med 2008;359:378–90. [PubMed: 18650514]
12. Kudo M, Finn RS, Qin S, Han KH, Ikeda K, Piscaglia F, Baron A, Park JW, Han G, Jassem J, Blanc JF, Vogel A, Komov D, Evans TRJ, Lopez C, Dutcus C, Guo M, Saito K, Kraljevic S, Tamai T, Ren M, Cheng AL. Lenvatinib versus sorafenib in first-line treatment of patients with unresectable hepatocellular carcinoma: a randomised phase 3 non-inferiority trial. Lancet 2018;391:1163–1173. [PubMed: 29433850]
13. Filmus J, Selleck SB. Glypicans: proteoglycans with a surprise. J Clin Invest 2001;108:497–501. [PubMed: 11518720]
14. Zhou F, Shang W, Yu X, Tian J. Glypican-3: A promising biomarker for hepatocellular carcinoma diagnosis and treatment. Med Res Rev 2018;38:741–767. [PubMed: 28621802]
15. Capurro MI, Xiang YY, Lobe C, Filmus J. Glypican-3 promotes the growth of hepatocellular carcinoma by stimulating canonical Wnt signaling. Cancer Res 2005;65:6245–54. [PubMed: 16024626]
16. Gao W, Kim H, Feng M, Phung Y, Xavier CP, Rubin JS, Ho M. Inactivation of Wnt signaling by a human antibody that recognizes the heparan sulfate chains of glypican-3 for liver cancer therapy. Hepatology 2014;60:576–87. [PubMed: 24492943]
17. Llovet JM, Chen Y, Wurmbach E, Roayaie S, Fiel MI, Schwartz M, Thung SN, Khitrov G, Zhang W, Villanueva A, Battiston C, Mazzaferro V, Bruix J, Waxman S, Friedman SL. A molecular signature to discriminate dysplastic nodules from early hepatocellular carcinoma in HCV cirrhosis. Gastroenterology 2006;131:1758–67. [PubMed: 17087938]
18. Libbrecht L, Severi T, Cassiman D, Vander Borght S, Pirenne J, Nevens F, Verslype C, van Pelt J, Roskams T. Glypican-3 expression distinguishes small hepatocellular carcinomas from cirrhosis, dysplastic nodules, and focal nodular hyperplasia-like nodules. Am J Surg Pathol 2006;30:1405–11. [PubMed: 17063081]
19. Wang XY, Degos F, Dubois S, Tessiore S, Allegretta M, Guttmann RD, Jothy S, Belghiti J, Bedossa P, Paradis V. Glypican-3 expression in hepatocellular tumors: diagnostic value for preneoplastic lesions and hepatocellular carcinomas. Hum Pathol 2006;37:1435–41. [PubMed: 16949914]
20. Capurro M, Wanless IR, Sherman M, Deboer G, Shi W, Miyoshi E, Filmus J. Glypican-3: A novel serum and histochemical marker for hepatocellular carcinoma. Gastroenterology 2003;125, 89–97. [PubMed: 12851874]
21. Yamauchi N, Watanabe A, Hishinuma M, Ohashi K, Midorikawa Y, Morishita Y, Niki T, Shibahara J, Mori M, Makuuchi M, Hippo Y, Kodama T, Iwanari H, Aburatani H, Fukayama M. The glypican 3 oncofetal protein is a promising diagnostic marker for hepatocellular carcinoma. Mod Pathol 2005;18:1591–8. [PubMed: 15920546]
22. Kandil D, Leiman G, Allegretta M, Trotman W, Pantanowitz L, Goulart R, Evans M. Glypican-3 immunocytochemistry in liver fine-needle aspirates : a novel stain to assist in the differentiation of benign and malignant liver lesions. Cancer 2007;111:316–22. [PubMed: 17763368]
23. Shirakawa H, Kuronuma T, Nishimura Y, Hasebe T, Nakano M, Gotohda N, Takahashi S, Nakagohri T, Konishi M, Kobayashi N, Kinoshita T, Nakatsura T. Glypican-3 is a useful

diagnostic marker for a component of hepatocellular carcinoma in human liver cancer. Int J Oncol 2009;34:649–56. [PubMed: 19212669]

24. Liu X, Wang SK, Zhang K, Zhang H, Pan Q, Liu Z, Pan H, Xue L, Yen Y, Chu PG. Expression of glypican 3 enriches hepatocellular carcinoma development-related genes and associates with carcinogenesis in cirrhotic livers. Carcinogenesis 2015;36:232–242. [PubMed: 25542894]
25. Miao HL, Pan ZJ, Lei CJ, Wen JY, Li MY, Liu ZK, Qiu ZD, Lin MZ, Chen NP, Chen M. Knockdown of GPC3 inhibits the proliferation of Huh7 hepatocellular carcinoma cells through down-regulation of YAP. J Cell Biochem 2013;114:625–31. [PubMed: 23060277]
26. Lee S, Xie J, Chen X. Peptides and peptide hormones for molecular imaging and disease diagnosis. Chem Rev 2010;110:3087–111. [PubMed: 20225899]
27. Zhang P, Cui Y, Anderson CF, Zhang C, Li Y, Wang R, Cui H. Peptide-based nanoprobes for molecular imaging and disease diagnostics. Chem Soc Rev 2018;47:3490–3529. [PubMed: 29497722]
28. Wang W, Hu Z. Targeting Peptide-Based Probes for Molecular Imaging and Diagnosis. Adv Mater 2019;31:e1804827. [PubMed: 30537222]
29. Lo A, Lin CT, Wu HC. Hepatocellular carcinoma cell-specific peptide ligand for targeted drug delivery. Mol Cancer Ther 2008;7:579–89. [PubMed: 18347144]
30. Du B, Han H, Wang Z, Kuang L, Wang L, Yu L, Wu M, Zhou Z, Qian M. Targeted drug delivery to hepatocarcinoma in vivo by phage-displayed specific binding peptide. Mol Cancer Res 2010;8:135–44. [PubMed: 20145035]
31. Line BR, Mitra A, Nan A, Ghandehari H. Targeting tumor angiogenesis: comparison of peptide and polymer-peptide conjugates. J Nucl Med 2005;46:1552–60. [PubMed: 16157540]
32. Juliano RL, Alam R, Dixit V, Kang HM. Cell-targeting and cell-penetrating peptides for delivery of therapeutic and imaging agents. Wiley Interdiscip Rev Nanomed Nanobiotechnol 2009;1:324–35. [PubMed: 20049800]
33. Chang DK, Lin CT, Wu CH, Wu HC. A novel peptide enhances therapeutic efficacy of liposomal anti-cancer drugs in mice models of human lung cancer. PLoS One 2009;4:e4171. [PubMed: 19137069]
34. Becker A, Hessenius C, Licha K, Ebert B, Sukowski U, Semmler W, Wiedenmann B, Grötzinger C. Receptor-targeted optical imaging of tumors with near-infrared fluorescent ligands. Nat Biotechnol 2001;19:327–31. 89. [PubMed: 11283589]
35. Achilefu S, Dorshow RB, Bugaj JE, Rajagopalan R. Novel receptor-targeted fluorescent contrast agents for in vivo tumor imaging. Invest Radiol 2000;35:479–85. [PubMed: 10946975]
36. Wester HJ, Kessler H. Molecular targeting with peptides or peptide-polymer conjugates: just a question of size? J Nucl Med 2005;46:1940–5. [PubMed: 16330555]
37. de Serres M, Ellis B, Dillberger JE, Rudolph SK, Hutchins JT, Boytos CM, Weigl DL, DePrince RB. Immunogenicity of thrombopoietin mimetic peptide GW395058 in BALB/c mice and New Zealand white rabbits: evaluation of the potential for thrombopoietin neutralizing antibody production in man. Stem Cells 1999;17:203–9. [PubMed: 10437983]
38. Tangri S, Mothé BR, Eisenbraun J, Sidney J, Southwood S, Briggs K, Zinckgraf J, Bilsel P, Newman M, Chesnut R, Licalsi C, Sette A. Rationally engineered therapeutic proteins with reduced immunogenicity. J Immunol 2005;174:3187–96. [PubMed: 15749848]
39. Fields GB, Noble RL. Solid phase peptide synthesis utilizing 9-fluorenylmethoxycarbonyl amino acids. Int J Pept Protein Res 1990;35:161–214. [PubMed: 2191922]
40. Bray BL. Large-scale manufacture of peptide therapeutics by chemical synthesis. Nat Rev Drug Discov 2003;2:587–953. [PubMed: 12815383]
41. Thurber GM, Schmidt MM, Wittrup KD. Antibody tumor penetration: transport opposed by systemic and antigen-mediated clearance. Adv Drug Deliv Rev 2008;60:1421–34. [PubMed: 18541331]
42. Wu AM, Senter PD. Arming antibodies: prospects and challenges for immunoconjugates. Nat Biotechnol. 2005;23:1137–46. [PubMed: 16151407]
43. Chauhan VP, Stylianopoulos T, Boucher Y, Jain RK. Delivery of molecular and nanoscale medicine to tumors: transport barriers and strategies. Annu Rev Chem Biomol Eng 2011;2:281–98. [PubMed: 22432620]

44. Heldin CH, Rubin K, Pietras K, Ostman A. High interstitial fluid pressure - an obstacle in cancer therapy. Nat Rev Cancer 2004;4:806–13. [PubMed: 15510161]
45. Smith A, Manoli H, Jaw S, Frutoz K, Epstein AL, Khawli LA, Theil FP. Unraveling the Effect of Immunogenicity on the PK/PD, Efficacy, and Safety of Therapeutic Proteins. J Immunol Res 2016;2016:2342187. [PubMed: 27579329]
46. Roessler S, Jia HL, Budhu A, Forgues M, Ye QH, Lee JS, Thorgeirsson SS, Sun Z, Tang ZY, Qin LX, Wang XW. A unique metastasis gene signature enables prediction of tumor relapse in early-stage hepatocellular carcinoma patients. Cancer Res 2010;70:10202–12. [PubMed: 21159642]
47. Ueda T, Honda M, Horimoto K, Aburatani S, Saito S, Yamashita T, Sakai Y, Nakamura M, Takatori H, Sunagozaka H, Kaneko S. Gene expression profiling of hepatitis B- and hepatitis C-related hepatocellular carcinoma using graphical Gaussian modeling. Genomics 2013;101:238–48. [PubMed: 23485556]
48. Carr JA, Franke D, Caram JR, Perkinson CF, Saif M, Askoxylakis V, Datta M, Fukumura D, Jain RK, Bawendi MG, Bruns OT. Shortwave infrared fluorescence imaging with the clinically approved near-infrared dye indocyanine green. Proc Natl Acad Sci U S A 2018:115:4465–4470. [PubMed: 29626132]
49. Maeda H, Wu J, Sawa T, Matsumura Y, Hori K. Tumor vascular permeability and the EPR effect in macromolecular therapeutics: a review. J Control Release 2000;65:271–84. [PubMed: 10699287]
50. Qin Z, Wang J, Wang Y, Wang G, Wang X, Zhou Z, Liu G, Gao S, Zhu L. Identification of a Glypican-3-Binding Peptide for In Vivo Non-Invasive Human Hepatocellular Carcinoma Detection. Macromol Biosci 2017;17:1600335.
51. Zhu D, Qin Y, Wang J, Zhang L, Zou S, Zhu X, Zhu L. Novel Glypican-3-Binding Peptide for in Vivo Hepatocellular Carcinoma Fluorescent Imaging. Bioconjug Chem 2016;27:831–9. [PubMed: 26850086]
52. Lee YL, Ahn BC, Lee Y, Lee SW, Cho JY, Lee J. Targeting of hepatocellular carcinoma with glypican-3-targeting peptide ligand. J Pept Sci 2011;17:763–9. [PubMed: 21976137]
53. Ishizawa T, Saiura A, Kokudo N. Clinical application of indocyanine green-fluorescence imaging during hepatectomy. Hepatobiliary Surg Nutr 2016;5:322–8. [PubMed: 27500144]
54. Nakaseko Y, Ishizawa T, Saiura A. Fluorescence-guided surgery for liver tumors. J Surg Oncol 2018;118:324–331. [PubMed: 30098296]
55. Jones AD, Wilton JC. Can intra-operative fluorescence play a significant role in hepatobiliary surgery? Eur J Surg Oncol 2017;43:1622–1627. [PubMed: 28320558]
56. Maeda H, Wu J, Sawa T, Matsumura Y, Hori K. Tumor vascular permeability and the EPR effect in macromolecular therapeutics: a review. J Control Release 2000;65:271–84. [PubMed: 10699287]
57. He K, Chi C, Li D, Zhang J, Niu G, Lv F, Wang J, Che W, Zhang L, Ji N, Zhu Z, Tian J, Chen X. Resection and survival data from a clinical trial of glioblastoma multiforme-specific IRDye800-BBN fluorescence-guided surgery. Bioengineering& Trans Med 20;e10182.
58. Thomas R, Chen J, Roudier MM, Vessella RL, Lantry LE, Nunn AD. In vitro binding evaluation of ^{177}Lu-AMBA, a novel ^{177}Lu-labeled GRP-R agonist for systemic radiotherapy in human tissues. Clin Exp Metastasis 2009;26:105–19. [PubMed: 18975117]
59. Joshi BP, Liu Z, Elahi SF, Appelman HD, Wang TD. Near-infrared-labeled peptide multimer functions as phage-mimic for high affinity, specific targeting of colonic adenomas in vivo, Gastrointestinal Endoscopy 2012; 2012;76:1197–206. [PubMed: 23022051]
60. Wang F, Duan X, Chen J, Gao Z, Zhou J, Wu X, Chang TS, Lee M, Li G, Nusrat A, Kuick R, Appelman HD, Wang TD. Integrated Imaging Methodology Detects Claudin-1 Expression in Premalignant Nonpolypoid and Polypoid Colonic Epithelium in Mice. Clin Transl Gastroenterol 2020;11:e00089. [PubMed: 31922993]

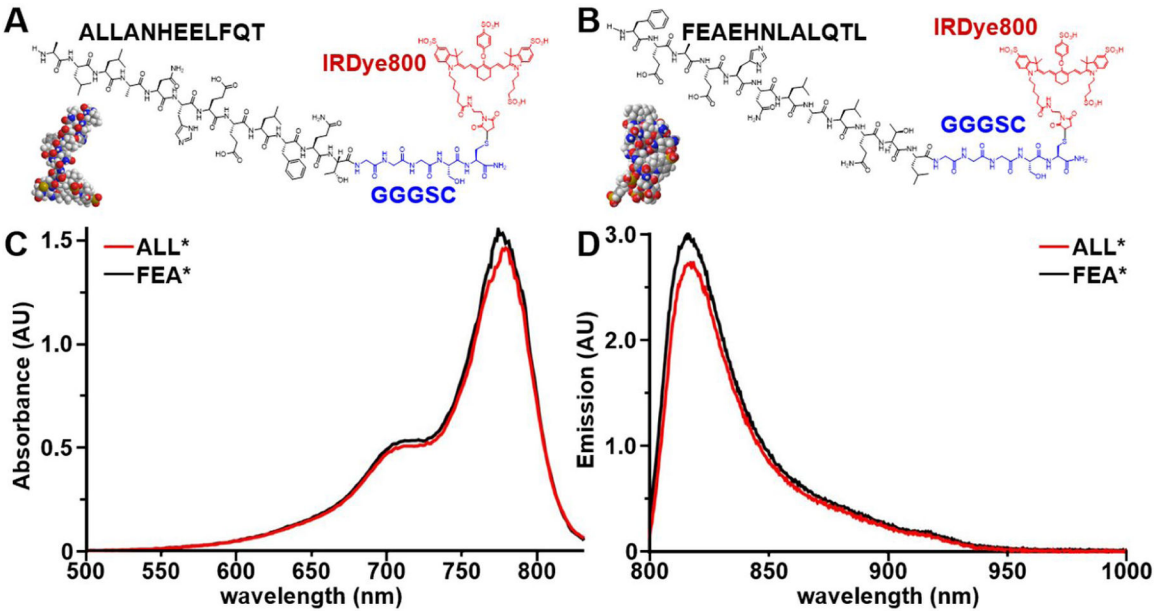

Fig. 1 –. Peptide specific for GPC3.

A) ALLANHEELFQT and **B**) FEAEHNLALQTL (scrambled control) are labeled with IRDye800 (red) via a GGGSC linker (blue) to prevent steric hindrance. 3D models show differences in biochemical structures. **C**) Peak absorbance and **D**) fluorescence emission wavelengths are found at λ_{abs} = 775 and λ_{em} = 816 nm, respectively.

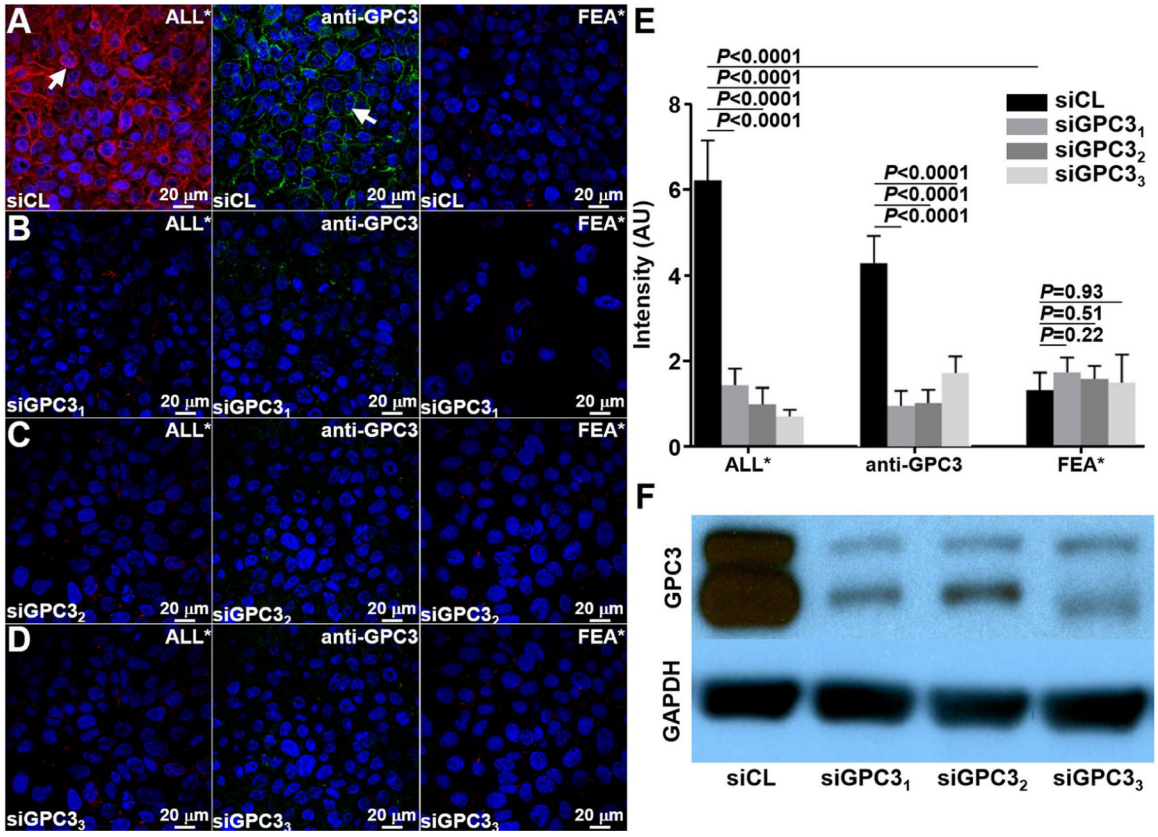

Fig. 2 –. Validation of specific peptide binding with knockdown.

A) ALL*-IRDye800 (red) and anti-GPC3-AF488 antibody (green) show strong binding in vitro to the surface (arrows) of human Hep3B HCC cells transfected with control siRNA (siCL). FEA*-IRDye800 shows minimal binding. **B**-**D**) Fluorescence intensities from the peptide and antibody are greatly reduced with knockdown of GPC3 expression in Hep3B cells transfected using 3 unique siRNAs. FEA*-IRDye800 shows minimal signal with all 3 siRNAs. **E**) A significant reduction in intensity is seen for ALL*-IRDye800 and anti-GPC3-AF488 for siCL versus siGPC3 transfected cells (siGPC3$_1$: 4.3 and 4.3-fold decrease, siGPC3$_2$: 6.1 and 4.0-fold decrease, and siGPC3$_3$: 8.7 and 2.5-fold decrease). FEA*-IRDye800 shows a non-significant difference with all 3 siRNAs. The intensity for ALL*-IRDye800 is significantly greater than that for FEA*-IRDye800 (4.7-fold increase). The siCL versus siRNA difference for ALL*-IRDye800 was significantly larger than the same difference for FEA*-IRDye800 (siGPC3$_1$: $P<1.0\times10^{-4}$, siGPC3$_2$: $P<1.0\times10^{-4}$, siGPC3$_3$: $P<1.0\times10^{-4}$). A one-way ANOVA was used to make the comparisons. Each result is an average of 6 independent measurements. **F**) Western blot shows GPC3 expression for all cells.

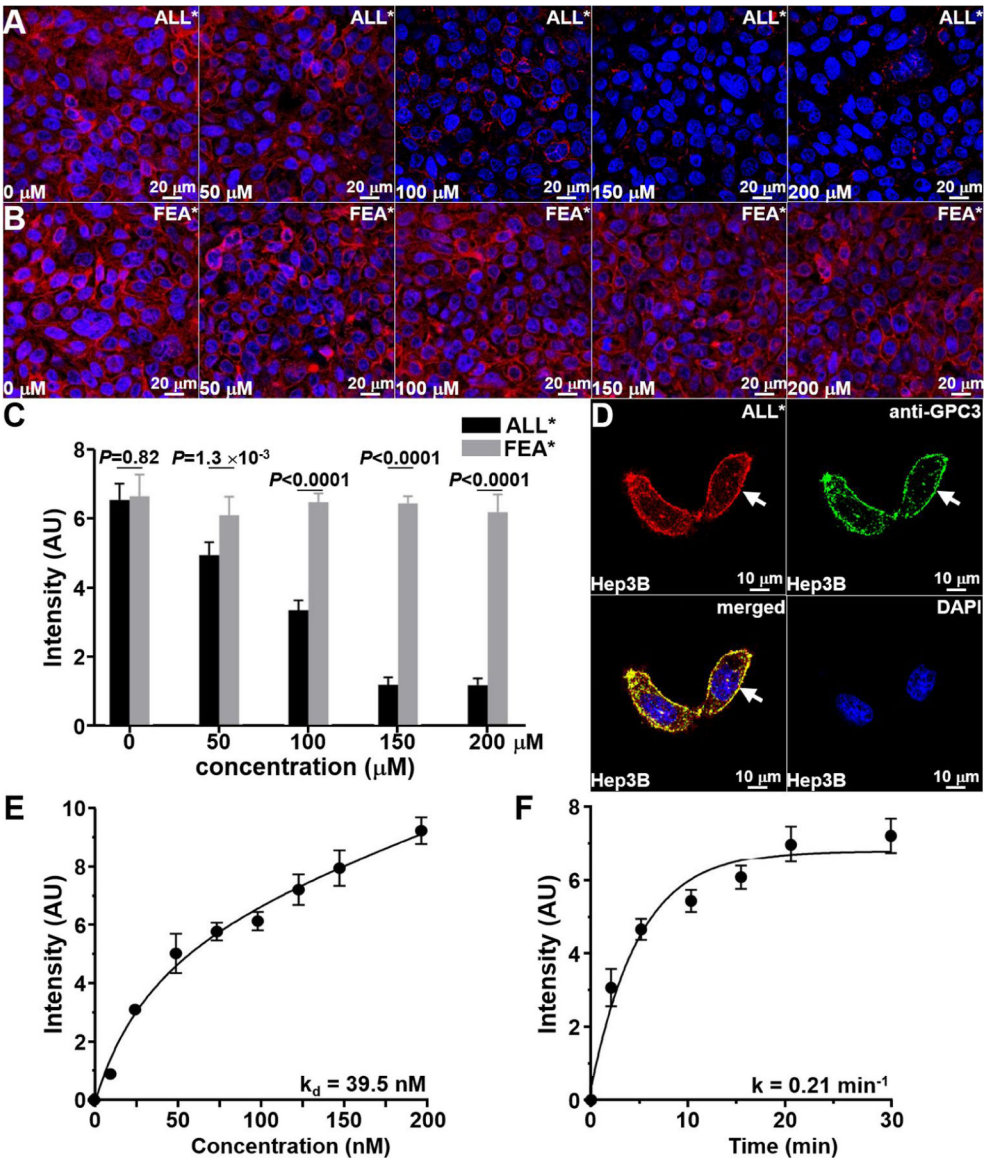

Fig. 3 –. Peptide characteristics.

Unlabeled **A**) ALL* and **B**) FEA* (control) were incubated with Hep3B cells in vitro to compete with ALL*-IRDye800 for binding. **C**) For ALL*, the mean (±SD) fluorescence intensities decreased significantly in a dose-dependent manner at concentrations of 50 μM and higher. FEA* showed no significant change at all concentrations. The *P*-values were determined using a two-way ANOVA with an interaction. Each result is an average of 6 independent measurements. **D**) Binding by ALL*-IRDye800 peptide and anti-GPC3 antibody to the surface of Hep3B cells co-localize (arrow) with a Pearson's correlation coefficient of $\rho = 0.71$ on the merged image. **E**) An apparent dissociation constant of $k_d = 39.5$ nM, $R^2 = 0.98$, and **F**) apparent association time constant of $k = 0.21\ min^{-1}$ (4.8 min), $R^2 = 0.95$, for binding of ALL*-IRDye800 to Hep3B cells were measured using flow cytometry. Results are representative of 3 independent experiments for each measurement.

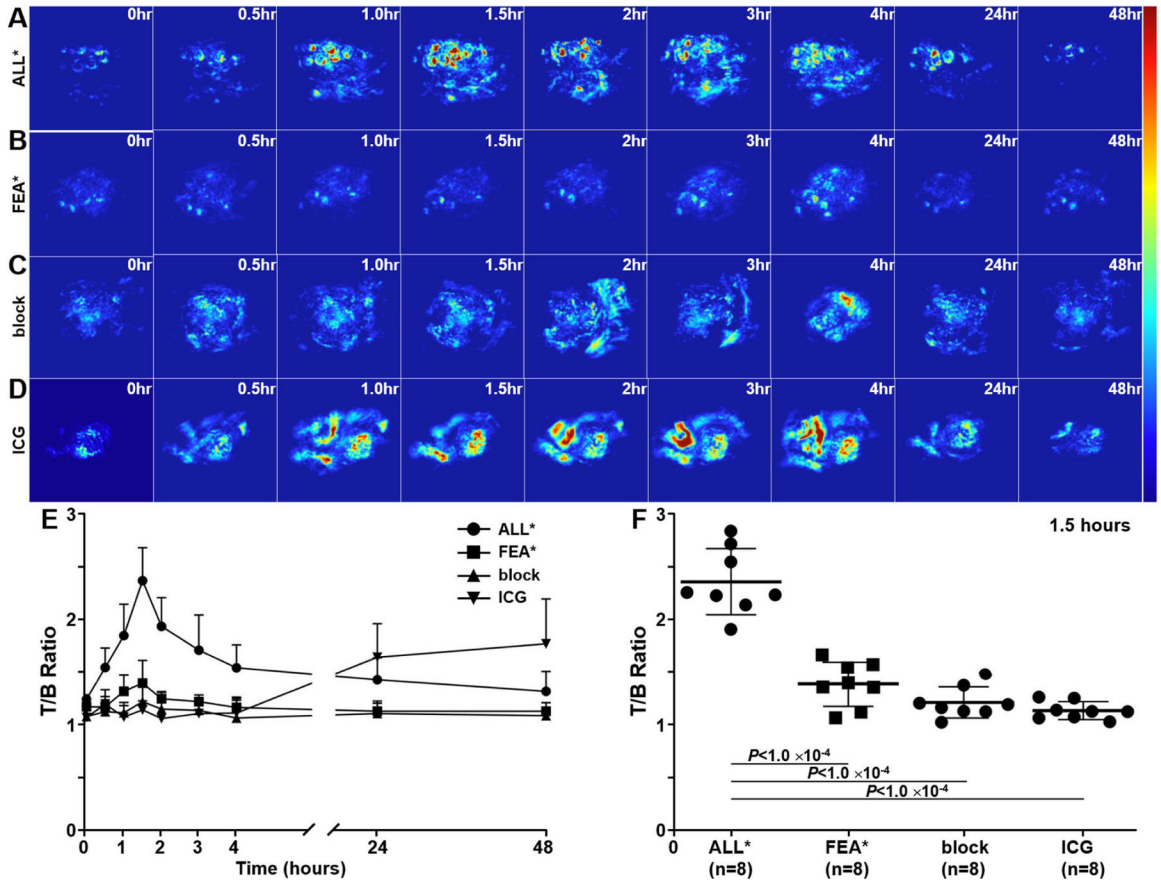

Fig. 4 –. In vivo photoacoustic imaging of HCC orthotopic tumors.

Representative photoacoustic images collected in vivo are shown from orthotopically-implanted human Hep3B (GPC3+) HCC xenograft tumors in immunocompromised mice from 0–48 hours following systemic administration of **A**) ALL*-IRDye800, **B**) FEA*-IRDye800 (control), **C**) ALL* (block), and **D**) ICG (control) with n = 8 animals per group. **E**) Quantified intensities shown peak uptake of ALL*-IRDye800 at 1.5 hours post-injection with clearance by ~24 hours. **F**) The mean (±SD) T/B ratio for ALL*-IRDye800 was significantly greater than that for FEA*-IRDye800, ALL* (block), and ICG with an increase of 1.7, 2.1, and 1.4-fold increase, respectively, respectively, at 1.5 hours post-injection. *P*-values were calculated using a one-way ANOVA model.

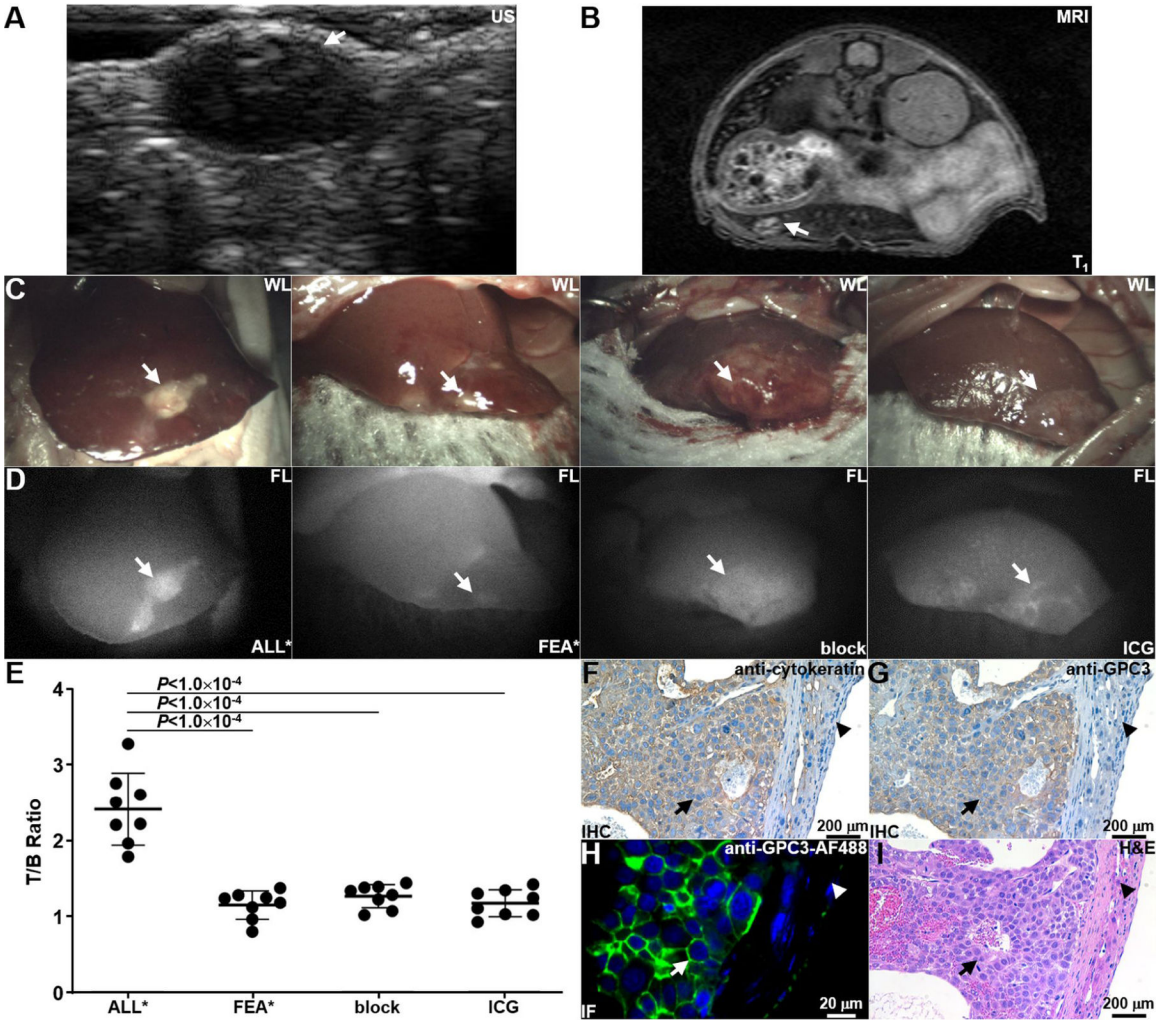

Fig. 5 –. In vivo laparoscopic imaging of HCC orthotopic tumors.

Representative **A**) ultrasound (US) and **B**) T_1-weighted MR images are shown of orthotopically-implanted HCC tumors (arrows). Representative **C**) white light (WL) and **D**) fluorescence (FL) images collected in vivo are shown at 1.5 hours post-injection of ALL*-IRDye800, FEA*-IRDye800, ALL* (block), and ICG with n = 8 animals per group. **E**) Quantified fluorescence intensities show the mean (±SD) T/B ratio for ALL*-IRDye800 was significantly greater than that for FEA*-IRDye800, ALL* (block), and ICG with 2.1, 2.1, and 1.9-fold increase, respectively. *P*-values were calculated using a one-way ANOVA model. **F**) Increased anti-cytokeratin reactivity shows presence of human HCC tumor (arrow) imbedded in mouse liver (arrowhead). **G**) Strong anti-GPC3 staining (arrow) confirms GPC3 expression in HCC. **H**) Bright fluorescence is seen on cell surface (arrow) in HCC. **I**) Corresponding histology (H&E) shows presence of human HCC tumor (arrow) implanted in mouse liver (arrowhead).

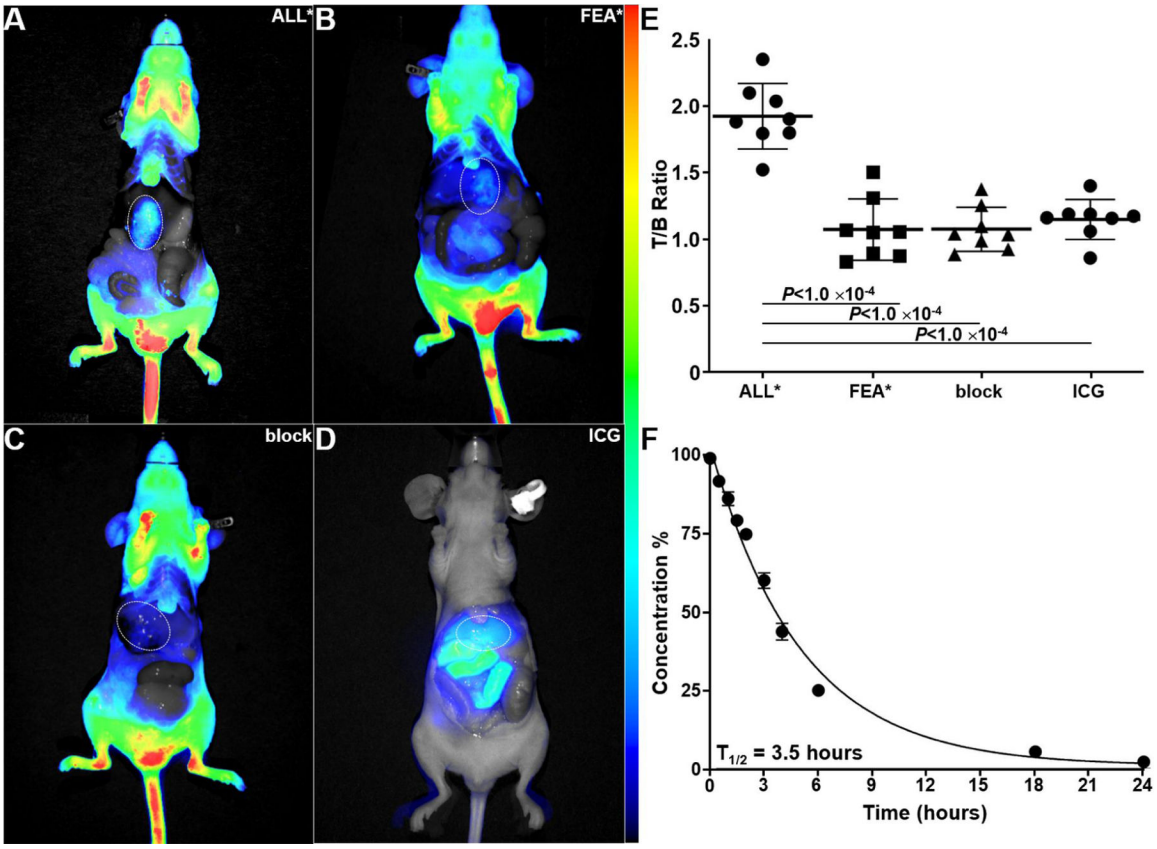

Fig. 6 –. In vivo whole body fluorescence images of HCC orthotopic tumors.

Representative images collected at 1.5 hours post-injection of **A**) ALL*-IRDye800, **B**) FEA*-IRDye800, **C**) ALL* (block), and **D**) ICG are shown with n = 8 animals per group. **E**) The mean (±SD) T/B ratio for ALL*-IRDye800 was significantly greater than that for FEA*-IRDye800, ALL* (block), and ICG with a 1.8, 1.7 and 1.8-fold increase, respectively. Pairwise *P*-values were calculated from an ANOVA model fit with terms for 4 conditions. **F**) Stability of ALL*-IRDye800 in mouse serum shows a half-life of $T_{1/2}$ = 3.5 hours, R^2 = 0.99.

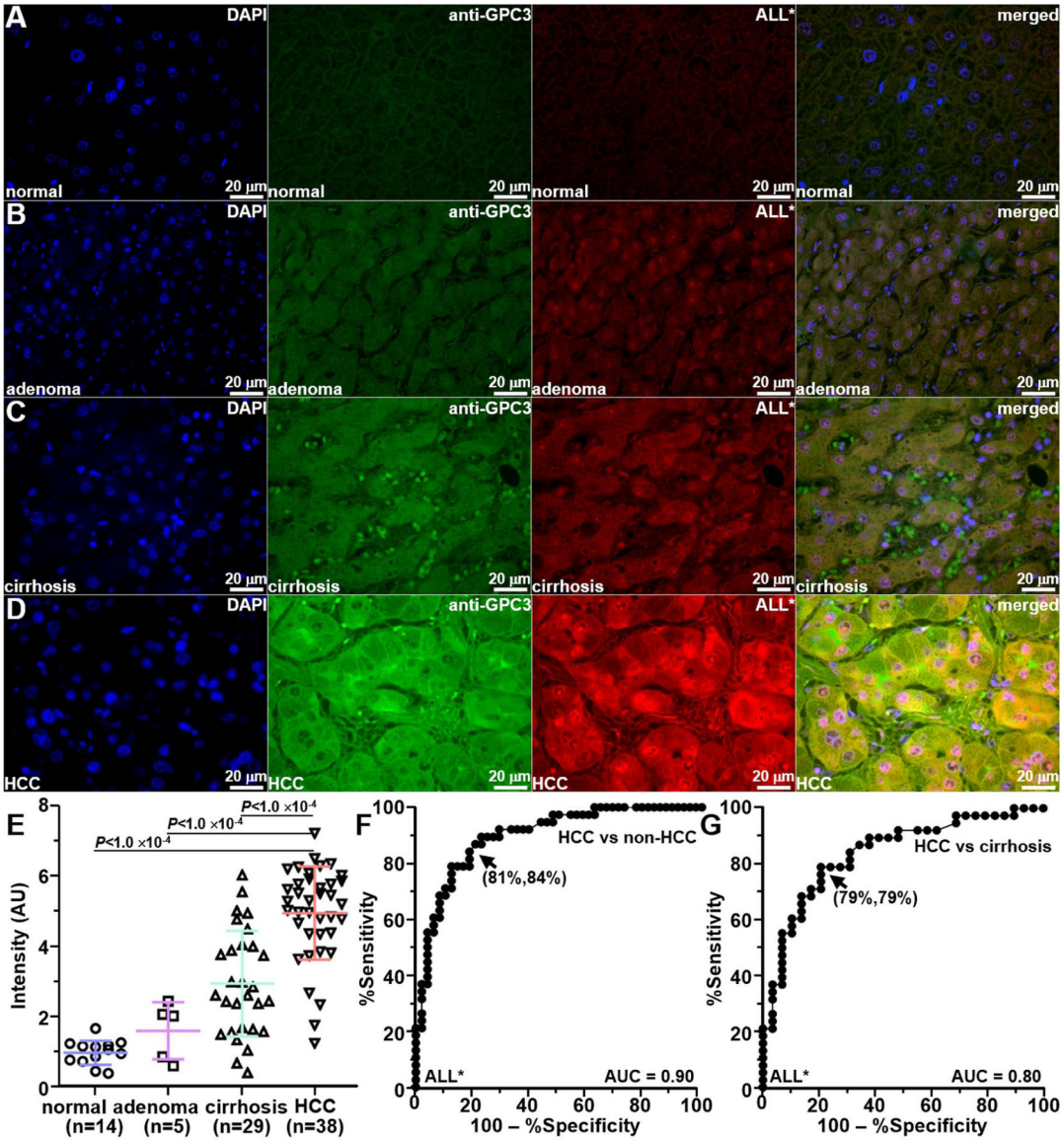

Fig. 7 –. Specific peptide binding to human HCC ex vivo.

On immunofluorescence, **A**) ALL*-IRDye800 (red) and anti-GPC3-AF488 (green) show minimal staining to normal human liver. A Pearson's correlation coefficient of ρ = 0.68 was measured from the merged image. DAPI image is shown. **B**) Mild staining is seen with peptide and antibody to adenoma with ρ = 0.82. **C**) Diffuse staining is observed for cirrhosis, with ρ = 0.72. **D**) Strong staining is visualized with HCC with ρ = 0.74. **E**) Quantified fluorescence intensities show a 5.3, 3.2, and 1.7-fold increase for HCC versus normal, adenoma, and cirrhosis. *P*-values are determined from data fit to one-way ANOVA model with terms for 4 conditions and n = 86 human specimens. **F**) ROC curve shows 81% sensitivity and 84% specificity for ALL*-IRDye800 to distinguish HCC from non-HCC with an area under curve of AUC = 0.90. **G**) ROC curve shows 79% sensitivity and 79% specificity to distinguishing HCC from cirrhosis with AUC = 0.80.